V. Gupta, J.L. Torero, J.P. Hidalgo (2021) Burning dynamics and in-depth flame spread of wood cribs in large compartment fires, **Combustion and Flame,** 228, 42-56.
https://doi.org/10.1016/j.combustflame.2021.01.031

Burning dynamics and in-depth flame spread of wood cribs in large compartment fires

Vinny Gupta*, Juan P. Hidalgo
School of Civil Engineering
The University of Queensland
Brisbane, QLD 4072, Australia

and

José L. Torero
Department of Civil, Environmental and Geomatic Engineering
University College London
London, WC1E 6BT, United Kingdom

(*) Corresponding Author: School of Civil Engineering
The University of Queensland
Brisbane, Queensland, 4072
Australia
Telephone: +61-424-032-837
e-mail: v.gupta@uq.edu.au

Full Length Paper

(Submitted to Combustion and Flame in October 2020)

Abstract

Wood cribs pervade the fire research literature as the chosen fuel load for testing within the built environment. As such, the underpinning knowledge of fire behaviour in compartments was developed from experiments using wood cribs in small compartments. Despite the apparent incomparability of porous fuel-beds such as cribs to real solid fuels in the built environment, the role of the fuel mass transfer number ("*B*-Number") in defining the compartment fire dynamics has received little attention. In the case of large open-plan compartments, the burning processes are strongly dependent on the relationship of the fuel nature and compartment geometry. To address these limitations, the physical processes in-depth and external to a spreading wood crib fire in a compartment are examined. A theory to couple these processes to a compartment is proposed and analogised into the classical "Emmons problem", leading to a definition of a total mass transfer number for a wood crib. Comparing the theory against data from a large-scale experiment shows that the wood crib approximates steady-state burning in two regimes: a fuel-bed-controlled regime and a momentum-controlled regime. The fuel-bed-controlled regime occurs when the burning and spread rates are governed by the processes internal to the crib, and the fire behaviour is therefore defined by the crib geometry. This regime is characterised by a fire that travels or grows slowly, with small external heat fluxes. The momentum-controlled regime occurs when the fire is fully-developed and the external heat fluxes are very large. Burning rates are controlled by the residence time, with the compartment fire dynamics defined by complex transport processes associated with the momentum-driven flows external to the crib. Transitions from the fuel-bed-controlled regime to the momentum-controlled regime are driven by accelerations in the flame spread rate along the surface of the crib leading to additional energy input mechanism that is used to raise the in-depth flame spread rate of the crib. It is hypothesised that the burning mechanisms of fuels with large mass transfer numbers, such as non-charring plastics, diverge significantly from wood cribs, and therefore extrapolating test data from wood cribs fires in compartments to real fuels must be done with extreme caution. Thus, the nature of the fuel is an important and unavoidable consideration when studying the fire dynamics of large open-plan compartments.

Keywords

Enclosure fires, diffusion flame, burning rate, flame spread, wood cribs, *B*- number

Nomenclature

A_s	Total exposed area of crib to air
$A_{s,t}$	Total top surface area of crib exposed to air
A_v	Total cross-sectional area of the crib vertical shafts
B	Mass transfer number
b	Stick thickness
C	Crib constant
c_p	Specific heat capacity
h	Enthalpy
h_c	Convective heat transfer coefficient
L_P	Pyrolysis length
$\dot{m}$	Mass flow rate
$\dot{m}''_b$	Total burning rate
$\dot{m}''_o$	Free crib burning rate
$\dot{m}''_r$	Radiative enhanced burning rate
N	Number of layers
n	Fitting exponent in Block's burning rate model
Pr	Prandtl number
Q	Total heat losses per unit mass of fuel produced
$\dot{q}''_{CV}$	Convective heat flux
$\dot{q}''_L$	Total heat losses at the surface of the fuel
$\dot{q}''_R$	Total radiative incident heat flux
$\dot{q}''_b$	Burning zone heat flux
$\dot{q}''_{b,f}$	Burning zone heat flux radiated ahead of the flame front
$\dot{q}''_e$	External heat flux
$\dot{q}''_f$	Flame heat flux
$\dot{q}''_{s,c}$	Solid-phase conduction
$\dot{q}''_{s,r}$	Surface re-radiation
s	Stick spacing
T	Temperature
u	Flow velocity (x-direction)
V_{BO}	Burnout front velocity
V_S	Flame front velocity
W	Fuel width
x	Stream wise co-ordinate
y	Co-ordinate perpendicular to the fuel surface
Y	Mass fraction
ΔH_C	Heat of combustion of oxygen
ΔH_P	Heat of pyrolysis

Greek Symbols

φ	Crib porosity factor
μ	Viscosity

ρ_h	Mass of heated crib per unit volume of fuel bed
τ	Shear stress
ψ	Geometric crib to floor ratio
ϕ'	Inverse opening factor
χ	Radiative fraction

Subscripts

A	Adiabatic
a	Air
f	Flame
id	In-depth within the crib
ig	Ignition
O_2	Oxygen
T	Total
s	Surface
sf	Top surface of the crib
0	At y=0
∞	Free stream
I	Convective mass transfer number
II	Radiative mass transfer number

1 Introduction

Experimental research in compartment and wildland fires over the past half-century have extensively applied wood cribs as an inexpensive and highly reproducible fuel source that is intended as a surrogate for real fuels. The advantage of crib structures is the self-enhancing effect due to the increased exposed surface area of wood within the structure and the resultant cross-radiation that enables for combustion of the crib to be sustained in the absence of an external heat flux. Crib structures were particularly useful for early compartment fire research because if the wood crib geometry was chosen correctly [1], it was guaranteed that the burning rate would reach a quasi-steady condition fast and continue to burn until almost full consumption of the fuel. This enabled easy characterisation of the fire and testing consistency when studying fully-developed fires [2]. Therefore, the underpinning knowledge of compartment fire dynamics is based on studies of fully-developed fires using wood cribs that were conducted in small-scale compartments in mostly air vitiated conditions [1,3–12].

Early compartment fire research linked the steady-state burning rate of the crib to the ventilation and geometry of a compartment provided that the openings were small [3-7]; a review of the fundamental principles is provided by Torero *et al*. [2]. These fires are often referred to as ventilation-controlled [6,7] as the rate of thermal decomposition of the fuel is regulated by the oxygen supply to the reaction zone. Thermal feedback from the hot smoke layer is limited by the oxygen concentration within the compartment [6] and therefore the burning mechanisms of the crib could be disregarded as the oxygen supply rate into the compartment is the controlling process of the fire. At larger scales, the fluid mechanics within the compartment are complex, and the burning rate is no longer limited only by the rate of oxygen supply into the compartment. Instead, heat transfer to the fuel, fuel geometry, fuel properties and thermal feedback from the compartment can all have a substantial influence on the burning rate. These fires are often referred to as fuel-controlled fires and fall outside any existing theory of compartment fires [6,7]. While this terminology might be slightly misleading as the fuel is not the sole parameter defining the fire behaviour [13,14], we will maintain it through this paper for consistency with earlier work [2,6,7].

A push for open floor plans in the built environment has motivated experimental fire research into fuel-controlled fires at very large-scale geometries recently [15–22]. Common to these experiments are porous wood crib fuel beds that are ignited at one end and allowed to freely propagate. The aim of these experiments was to measure the spread rates, heat release rates, and the thermal solicitation to the boundaries (i.e. the structure). The geometry of the compartment is sufficiently large such that the fires are not ventilation-controlled and measured outputs strongly depend on the burning properties of the fuel. Despite this dependence, there has been little consideration of how the spread and burning of wood cribs determine the behaviour of the fire. This is particularly problematic as the structure of cribs allows for spread and burning to occur in-depth as a porous medium, which has not been studied in detail.

Previous studies on propagating and non-propagating wood crib fires have been mostly experimental and were conducted in unconfined atmospheres [23–29]. Theoretical developments on free burning crib fires have either focused on the process above the crib or within the crib, with little consideration on the coupling of the two [30–35]. In an enclosed atmosphere, external heating on the fuel occurs from the positive feedback loop as more energy is introduced [36]. Then, the coupling of the processes inside and above the crib becomes an unavoidable consideration. This has never been studied in detail.

Measured spread rates from compartment fire experiments are usually limited to the surface of the crib, however, surface spread can differ to the in-depth spread rates within the crib. Consequently, the energy released by spreading cribs fires during large-scale experiments is not well characterised. The Malveira Fire Test (MFT) is of interest because of the high density of instrumentation that enabled the measurement of burning rate, spread rates and external heat fluxes over a long continuous wood crib fuel-bed [18]. It was shown that the thermal fields generated by the fire are associated with the propagation velocity of the flame front ($V_{\mathrm{S,sf}}$) along the surface of the fuel and the propagation velocity of the burnout front (V_{BO}). The ratio of the two quantities was classified as the fire spread mode ($V_{\mathrm{S,sf}}/V_{\mathrm{BO}}$) and three modes were identified from the experiment:

- Mode 1: a fully-developed fire where $V_{\mathrm{S,sf}}/V_{\mathrm{BO}} \to \infty$
- Mode 2: a spreading fire where $V_{\mathrm{S,sf}}/V_{\mathrm{BO}} > 1$
- Mode 3: a travelling fire where $V_{\mathrm{S,sf}}/V_{\mathrm{BO}} \approx 1$

These modes were artificially simulated using controlled gas burners by Hidalgo *et al.* [37] and the compartment energy balance for each mode was subsequently calculated by Gupta *et al*. [14]. It was found that each mode of $V_{\mathrm{S,sf}}/V_{\mathrm{BO}}$ induced a characteristic distribution of the energy within the compartment. The mechanisms controlling $V_{\mathrm{S,sf}}/V_{\mathrm{BO}}$ for spreading wood crib fires has recently been studied by Gupta *et al*. [19] using experimental data collected from the MFT [18], Edinburgh Tall Building Fire Tests campaign [37], and the Guttasjön Fire Tests campaign [17]. $V_{\mathrm{S,sf}}$ was considered as a surface spread property and was found to be controlled by external radiation from the compartment ($\dot{q}''_{\mathrm{e}}$) that preheats the fuel and the forward flame heat flux ($\dot{q}''_{\mathrm{f,f}}$). These quantities were shown to be dependent on the compartment geometry, ventilation conditions and thermal properties of the fuel. The burnout front velocity, V_{BO} was shown to have a weak dependence to external radiation, $\dot{q}''_{\mathrm{e}}$ and was approximately a constant. The magnitude of V_{BO} is controlled by the characteristic burnout time and is, therefore, a function of the burning rate (per unit area) $\dot{m}''_{\mathrm{b}}$ and the total mass of the fuel per unit area. A key aspect not considered, and one that is unique to porous fuels such as cribs is the propagation of the burning zone beneath the surface of the crib which determines the total energy released into the compartment.

Understanding the physical mechanisms controlling the burning and spread of fires in cribs is necessary to evaluate the role of fuel geometry on the fire behaviour in large compartment fires. In the absence of this information, it is not possible to explain compartment fire dynamics in fires that are not ventilation-controlled. This work systematically evaluates the processes governing the burning dynamics and in-depth flame spread of wood crib fires in large compartments. Regimes of crib burning behaviour in large compartments are identified and defined in terms of a non-dimensional total mass transfer number B_{T}. The theory is evaluated with data collected from a large-scale compartment fire experiment to demonstrate the limit states for the burning regimes and the mechanisms that enable transitions from one regime to another. Implications of these regimes to the definition of the compartment fire dynamics will be discussed.

2 Physics of cribs

2.1 Physical description

A detailed analysis of the phenomena occurring inside and above the crib is necessary for extracting the mechanisms controlling the fire spread and burning rates when subject to external radiative

heating from the smoke layer and physical boundaries of the compartment. Figure 1 shows the physical dimensions of the three-dimensional crib structure. The crib comprises N layers of sticks of a square cross-section of thickness b (cm). Sticks are spaced equally by s (cm), and the crib is generally designed such that the top layer of sticks is in the direction of spread along the length L of the crib.

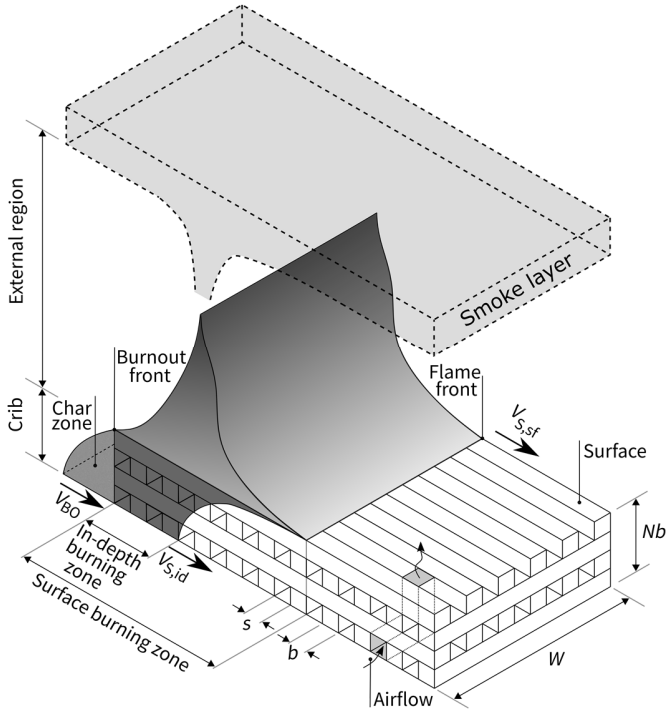

Figure 1: Schematic diagram of a spreading fire through a crib fuel structure in a compartment with key physical dimensions and characteristics.

The porous nature of the fuel structure allows for heat and mass transfer to occur both inside and above of the crib. The region inside of the porous media of the crib will be referred to as the in-depth region, while the region above the surface of the crib will be referred to as the external region. Advective transport occurs in-depth in the crib, and therefore the crib can burn and spread in-depth within the porous media. External to the crib, heat is transferred to the top surface of the crib through convection and radiation from the flame and radiation from external heat sources such as the smoke layer or the compartment boundaries. Consequently, the surface and in-depth burning zones are demarcated. The illustrated profile of the burning zone in Fig. 1 is only intended to be indicative and it is assumed from observations of the reported experiments in the literature [15,19]. An analysis of the heat and mass transfer mechanisms for a crib must treat the in-depth and external processes independently.

2.2 Processes in-depth to the crib

Once the crib is ignited and burning, air is transported into the crib through the crib shafts along the open sides. Mixing and combustion are assumed to occur infinitely fast in the open vertical shafts of the crib structure. Hot combustion gases are transported upwards by buoyancy through the vertical shafts, providing additional heat that is used to pyrolyse more fuel. The flue from the vertical shaft is ejected through the total area of the open vents, A_v at the surface of the crib. The

available fuel for combustion is determined by the surface area of fuel in the crib that is exposed to the flow, A_s. From this physical description of the crib, the rate of thermal decomposition of the fuel, or burning rate, $\dot{m}_b''$ is determined by the heat and mass transport inside of the vertical shaft.

The physical dimensions of the crib are important, as these define the porosity of the fuel. The crib porosity determines the mass flow rate of air, $\dot{m}_a$ flowing into the crib and is therefore responsible for the mass fraction of oxygen, Y_{O_2} in each vertical shaft that is available for combustion within the crib structure. Based on this concept, the crib porosity factor, φ is defined by the ratio of air-to-fuel mass flow rates, $\dot{m}_a/\dot{m}_b$ inside the vertical shafts. Experimental studies on free burning wood crib fires show that the burning rate is a strong function of φ [25,26,28,34,35,38,39]. Based on the porosity factor, three free burning regimes were identified: (1) a diffusion-limited combustion regime where the burning rate is controlled by porosity, (2) a free combustion regime where the burning rate is independent of the crib porosity and instead controlled by the thickness of the sticks, and (3) a non-sustained combustion regime where the crib porosity is too high to maintain combustion. It was found from the experimental data that for cribs, the steady-state burning rate follows the relation $\dot{m}_b'' \propto b^{-n}$, where b is the thickness of a single stick and n is a fitting exponent [25]. Heskestad assumes that the mass flow rate of air entering the crib follows the relation $\dot{m}_a \propto A_v s^{1/2}$, and sets $n = 0.5$ to propose the following expression for the crib porosity factor that best fit the experimental data across the burning regimes [9]:

$$\frac{\dot{m}_b}{\dot{m}_a} \propto \frac{\dot{m}_b}{A_s b^{-0.5}} = f\left[\left(\frac{A_v}{A_s}\right) s^{0.5} b^{0.5}\right] = f(\varphi) \tag{1}$$

where $\dot{m}_b$ is the mass loss rate (g/s), A_s is the total surface area of wood exposed to air (cm^2), b is the thickness of a single stick of wood (cm), A_v is the total cross-sectional area of the vertical shafts in the crib (cm^2), s is the spacing between each stick (cm), and φ is the porosity factor (cm).

The definition of the porosity factor in Eq. (1) is meaningful as it shows that, outside the quenching regime, if the flame is expected to burn with constant stoichiometry then the burning rate can be formulated because the air-fuel ratio is constant. Therefore, the existence of a variable porosity factor is the realisation that stoichiometry is not constant, and is simply an estimate of the flow of air through the crib which defines whether the combustion is fuel-rich or stoichiometric leading to the regimes identified by Gross [25].

Theoretical models to solve the burning rates for both regimes were developed by Block [38]. Using the porosity factor, Block defined a porosity-controlled regime and an open regime. Heskestad applied Eq. (1) to Block's data and showed that separation of the two regimes occurs at approximately $\varphi \approx 0.75$ cm [9]. An analogy for the burning of a crib is formulated based on a single vertical shaft that is modelled as a very rough-walled, porous tube. In the porosity-controlled regime ($\varphi < 0.75$ cm), the burning rate is controlled by the rate at which air can be drawn into the shaft and is calculated as a function of the geometric and physical properties of the crib [38]. In the open regime, the spacings do not have any effect on the burning rate, and the shafts are regarded as well-ventilated as the residence time for airflow is small. The burning rate is approximated by the number of vertical surfaces in a shaft that is exposed to air with reacting boundary layers established over each surface. For small sticks, it is reasonable to assume that heat transfer is dominated by convective and diffusive transport such that the flame is optically-thin and radiation from the flame is negligible. The two mechanisms of heat transfer to the fuel surfaces inside the crib responsible for its free burning rate are: (1) convective heat transfer from the flame, and (2)

radiative heat transfer exchanged from other burning sticks. The energy balance at the vertical surface of an exposed stick within the crib can be expressed as

$$\dot{m}''_{\mathrm{b}}\Delta H_{\mathrm{P}} = \dot{q}''_{\mathrm{CV}} + \dot{q}''_{\mathrm{R}} - \dot{q}''_{\mathrm{L}} \tag{2}$$

where ΔH_{P} is the heat of pyrolysis, $\dot{q}''_{\mathrm{CV}}$ is the convective heat flux from the flame to the fuel, $\dot{q}''_{\mathrm{R}}$ is the incident radiative heat flux from other burning sticks and the flame, and $\dot{q}''_{\mathrm{L}}$ are the heat losses at the surface of the fuel.

The ratio of the left and right-hand sides of Eq. (2) results in the definition of a mass transfer number, or "B-number" which is generalised as

$$B = \frac{\text{Energy available to pyrolyse fuel}}{\text{Energy required to pyrolyse fuel}} \tag{3}$$

For burning wood in the absence of external heat, convective heat transfer from the flame supports pyrolysis of the fuel and leads to the definition of the first mass transfer number that is specific to convection:

$$B_{\mathrm{I}} = \frac{\dot{q}''_{\mathrm{CV}}}{\dot{m}''_{\mathrm{b}}\Delta H_{\mathrm{P}}} \tag{4}$$

For charring materials such as wood, B decays transiently as the net heat flux at the pyrolysis front is dampened by the growing char layer thickness. Flame extinction has to occur when the convective heat flux is not large enough, therefore $B_{\mathrm{I}} < 1$. To sustain pyrolysis, the crib structure must deliver an external radiative heat flux to the surface of the fuel, and a second mass transfer number for radiation can be defined:

$$B_{II} = \frac{\dot{q}''_{\mathrm{R}}}{\dot{m}''_{\mathrm{b}}\Delta H_{\mathrm{P}}} \tag{5}$$

The total mass transfer for the crib is determined by combining B_{I} and B_{II}. It is clear for cribs that B_{II} is a necessary factor that drives the burning and flame spread behaviour of the crib, and it is necessary to describe the process of radiative heat transfer in-depth within the crib. Underneath the flames, the charred surface of each stick undergoes smouldering combustion (solid-phase oxidation) which radiates with a high emissivity [40]. The radiative heat received by each stick is determined by the radiation mean free path inside the crib. It can be assumed that radiation is conserved in-depth within the crib under the implication that radiation incident on each exposed surface of wood is larger than the surface re-radiation losses, $\dot{q}''_{\mathrm{s,r}}$. Consequently, the crib structure insulates heat in-depth and minimises the heat losses. Assuming that the shape of the burning sticks does not change significantly during degradation, the radiative heat flux inside the burning zone that is incident on all exposed surfaces can be treated as constant and lumped as $\dot{q}''_{\mathrm{b}}$. Radiation transferred from the smouldering char zone left in the wake of the burnout front to the burning zone can be treated as negligible based on the experimental results of McCarter and Broido who found a minimal effect of the char zone on the crib burning rate [41].

Once a flame is established, heat is transferred forward in-depth within the crib to the virgin fuel. If the local burnout time ($t_{\mathrm{BO}} = m''/\dot{m}_{\mathrm{b}}''$) is greater than the ignition delay time of the fuel ahead of the burning zone, the fire will continue spreading. In-depth flame spread in cribs has received little attention, with few studies focused on measuring the spread rates of freely propagating fires [24,27,33,41–43]. These studies showed that under quiescent air conditions, flame spread is of the opposed type and within the crib, the flame front is uniform vertically in-depth. This indicates that radiation from the flame above the crib does not contribute to faster surface spread rates [24]. McCarter and Broido [41] and Thomas [27] showed that changing the flame height or shielding the flames above the crib had little effect on the crib burning and spread rate. Thomas attributes this to the flame established above the crib being optically-thin, therefore radiative heat transfer from the flame to the fuel is negligible. Convective heat transfer to the fuel from the flames above the crib was assumed negligible because the flames are dominated by buoyancy and do not tilt toward the fuel. If the direction of in-depth spread is opposed to the airflow, the principal mechanism of fire spread is by radiative feedback within the crib that transfers heat by radiation through the porous media to the leading edge of the burning zone. The forward heat flux from the burning zone $\dot{q}''_{\mathrm{b,f}}$ is used to compensate for convective heat losses and to raise the temperature of the cross-sectional area of unburned crib from ambient to the ignition temperature. Thomas proposed the following expression to describe energy conservation at the leading edge of the burning zone

$$\rho_{\mathrm{h}} c_{\mathrm{p,s}} (T_{\mathrm{ig}} - T_{\mathrm{s}}) V_{\mathrm{S,id}} = \dot{q}''_{\mathrm{b,f}} - h_{\mathrm{c}} (T_{\mathrm{s}} - T_{\infty}) \tag{6}$$

where $V_{\mathrm{S,id}}$ is the in-depth flame spread velocity (which is assumed to be uniform with the surface flame spread rate), ρ_{h} is the mass of crib heated to ignition per unit volume of fuel bed, $c_{\mathrm{p,s}}$ is the specific heat capacity of the solid, T_{ig} is the ignition temperature, T_{s} is the solid temperature which Thomas assumes as ambient, $\dot{q}''_{\mathrm{b,f}}$ is radiative heat flux from the burning zone that is radiated forward to the unburned fuel, and h_{c} is a convective heat transfer coefficient.

Following the approach of Thomas, $V_{\mathrm{S,id}}$ can be solved from Eq. (6) for thermally-thick wooden sticks with varying crib geometries [31,33]. The solution to $V_{\mathrm{S,id}}$ assumes that $T_{\mathrm{s}} \approx T_{\infty}$ prior to the arrival of the flame front, and therefore the controlling mechanism of flame spread is by radiative heat transfer within the crib. Thomas fitted $\dot{q}''_{\mathrm{b,f}}$ to experimental data and found that the magnitude of $\dot{q}''_{\mathrm{b,f}}$ ranges within 60-80 kW/m^2 for high-porosity cribs [33]. It is important to emphasise that $\dot{q}''_{\mathrm{b,f}}$ is determined by the magnitude of the heat flux originating from the in-depth burning zone ($\dot{q}''_{\mathrm{b}}$). Both parameters are properties of radiation heat transfer inside the crib and therefore are related to the mass transfer number B. An additional flame spread mechanism appears in Eq. (6) if T_{s} is modified at the surface of the crib by external heating prior to the arrival of the flame front. This leads to a decoupling of the surface flame spread velocity ($V_{\mathrm{S,sf}}$) and the in-depth flame spread velocity ($V_{\mathrm{S,id}}$) as the mechanism that drives the surface spread rate is external to the crib. The assumption by Thomas eliminates this possibility, and therefore consideration of the physical processes external to the crib is necessary.

2.3 Processes external to the crib

Due to the strong buoyancy forces in the vertical shafts, fuel is transported into the flue above the crib and burns as a flame above the crib. The flame height is determined as a function of the total mass flux of pyrolyzates generated from the in-depth burning zone [30]. Measurements of the radiative fraction by McCarter and Broido show that the radiative fraction χ of the flames above the

crib can be approximated such that $\chi \approx 0.21$ [41]. Therefore, the majority of the energy released from the flames is through convection, and the resultant thermal feedback from the flame onto the fuel is negligible ($\dot{q}''_{\mathrm{f}} \approx 0$) assuming the flame volume is not substantially large. In an enclosed environment such as a compartment, if the geometry permits, hot gases and smoke can accumulate along the ceiling and enable a thermal feedback mechanism onto the top surface of the fuel by an external heat flux, $\dot{q}''_{\mathrm{e}}$ [19].

The external heat flux from compartment boundaries, smoke layer and flame volume preheats the unburned crib surface ahead of the flame front beyond an ambient temperature ($T_{\mathrm{s,sf}} > T_{\infty}$). Under this condition, flame spread rates in-depth to the crib and flame spread rates along the surface of the crib can no longer be considered to have a direct relationship because there is an independent variable that is the external heat flux. Larger magnitudes of $\dot{q}''_{\mathrm{e}}$ and longer preheating times from the smoke layer onto the crib surface lead to faster surface spread rates [19]. The surface burning area receives thermal feedback from the smoke layer that not only accelerates spread, but it also enhances the total burning rate. The enhanced burning rate by radiation adds a further mechanism for energy production in the compartment and is given by

$$\frac{\dot{m}_{\mathrm{r}}}{A_{\mathrm{s,t}}} = \frac{\dot{q}''_{e}}{\Delta H_{\mathrm{P}}} \tag{7}$$

where $\dot{m}''_{\mathrm{r}} = \dot{m}_{\mathrm{r}}/A_{\mathrm{s,t}}$ and is the burning rate due to external heating to the top surface area ($A_{\mathrm{s,t}}$) of the crib. Surface heat losses associated with the radiative enhanced burning rate are incorporated into an effective value for the heat of pyrolysis (ΔH_{P}).

As more energy is introduced into the compartment from the surface burning zone, a feedback mechanism occurs as $\dot{q}''_{\mathrm{e}}$, $V_{\mathrm{S,sf}}$, $A_{\mathrm{s,t}}$ and $\dot{m}''_{\mathrm{r}}$ evolve as a function of time because of the heating of the compartment and smoke layer. This implies that the unburned crib is transiently heated by an evolving $\dot{q}''_{\mathrm{e}}$. If T_{s} remains below the ignition temperature, T_{ig}, surface spread is controlled by the preheating time. The limiting condition for spread occurs when sufficient energy is introduced into the compartment leading to reduced preheating times, however, the magnitude of $\dot{q}''_{\mathrm{e}}$ is large. At this point, $T_{\mathrm{s}} \approx T_{\mathrm{ig}}$ at the arrival of the flame, leading to rapid flame spread ($V_{\mathrm{S,sf}}/V_{\mathrm{BO}} \gg 1$) across the remaining unburned fuel along the surface of the crib. Observations from large-scale experiments in this region show complete involvement of the crib in the fire shortly after rapid flame spread along the surface of the crib occurs [18,19].

In the region where $\dot{q}''_{\mathrm{e}}$ is large, the magnitude of $V_{\mathrm{S,sf}}$ and $\dot{m}''_{\mathrm{r}}$ leads to a scenario where the external heating can no longer be ignored and significantly influences the mass transfer number. Furthermore, it can be expected that as $V_{S,sf}/V_{BO} \rightarrow \infty$ and the entirety of the fuel is involved in the fire, the flame transitions to being optically-thick that radiates with a large emissivity and radiative fraction χ due to the very large flame volume [32]. In this case, the radiative feedback from the flame onto the fuel by $\dot{q}''_{\mathrm{f}}$ must be considered in the definition of B_{II}. To examine the role of the external heating for cribs, Thomas modified the energy balance from Eq. (6) to include radiation from the flame and applied a scaling analysis for a crib fire in still air [33]. Thomas showed two steady-state spread regimes, corresponding to a slow spread regime where fire spread is controlled by radiative heat transfer in-depth within the crib from the high emissivity burning zone, and a fast spread regime where fire spread is controlled by the radiative heat transfer external to the crib from the highly emissive flames. In the latter regime, $\dot{q}''_{\mathrm{f}}$ dominates the in-depth spread rate. Thomas assumes that the fire front is always uniform, implying that the spread rates in-depth and along the surface of the crib are in equilibrium ($V_{\mathrm{S,id}} = V_{\mathrm{S,sf}}$) and are linked to the fuel burning rate.

This assumption is untenable if a radiative contribution from the compartment onto the crib surface is established.

The theory of Thomas was established on the basis that the fire burns in an unconfined atmosphere with infinitely long length-scales. In this case, the transition of regimes is associated with the onset of the fire reaching a critical length-scale, allowing for a transition to an optically-thick flame with a considerably larger radiative fraction. Under these conditions, heat transfer from the flame by $\dot{q}''_{\mathrm{f}}$ cannot be neglected. This theory can be extended to smaller length-scales as external heating onto the crib by $\dot{q}''_{\mathrm{e}}$ can induce a transition from one regime to another. In this case, the transition is purely driven by surface spread and the contribution from $\dot{q}''_{\mathrm{f}}$ is a consequence of attaining rapid flame spread along the crib surface that modifies the energy balance in-depth within the crib. Figure 2 shows a diagram of the heat transfer pathways at the flame leading edge that can lead to different regimes of behaviour and the transition to a fully-developed fire.

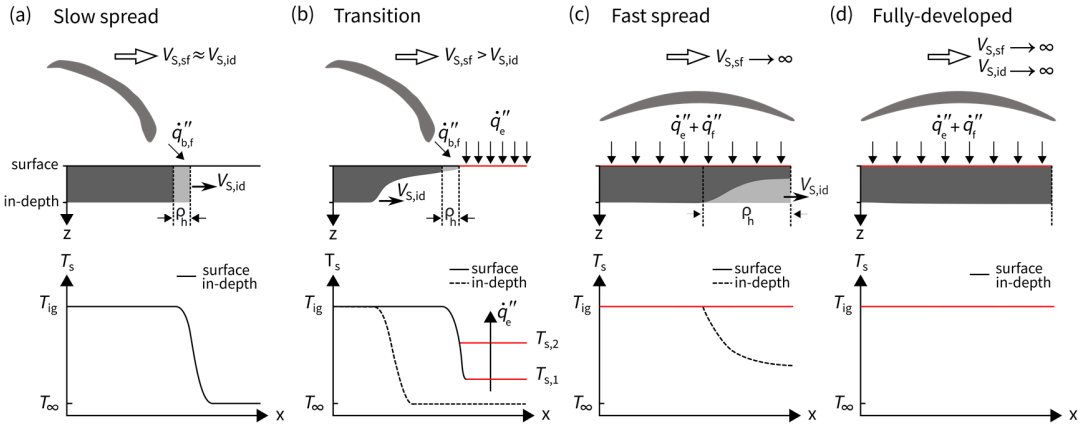

Figure 2: Theorised surface and in-depth temperature profiles leading to each theorised regime (a-d) as a function of an increasing external heat flux ($\dot{q}''_{e}$).

Two steady-state regimes of behaviour can be theorised in terms of $\dot{q}''_{\mathrm{e}}$. In the first regime, $\dot{q}''_{\mathrm{e}}$ is small and the burning and spread rates are governed by in-depth radiative heat transfer within the porous media of the crib (Fig. 2a). The slow spread regime is equivalent to the free burning crib. An unsteady transition from the slow spread regime to the fast spread regime occurs as $\dot{q}''_{\mathrm{e}}$ increases during the evolution of the fire due to the build-up and heating of the smoke layer, thus leading to faster surface spread (Fig. 2b) [19]. At the instance that the crib surface temperature ahead of the surface flame front approximates the ignition temperature, rapid flame spread across the surface is attained (Fig. 2c), leading to the second steady-state regime that is dominated by heat transfer external to the porous media of the crib. This regime corresponds to large values of $\dot{q}''_{\mathrm{e}}$ and a strong contribution from the flame by $\dot{q}''_{f}$ that governs the burning rate and must be accounted for in the energy balance for the in-depth region of the crib (Fig. 2d). This additional mechanism accelerates the in-depth flame spread rate suddenly. In both steady-state regimes, the mechanisms that deliver burning and in-depth spread rates and their respective magnitudes are determined by the crib mass transfer number.

2.4 Total mass transfer number for a crib

A mass transfer number for a wood crib is desired to evaluate the role of an external heat flux from the compartment on the crib burning dynamics and in-depth flame spread. The crib burning rate is analogous to the combustion of the vertical surface of a single stick exposed to forced airflow inside

a shaft of the crib, and therefore the reacting flow approximates a boundary layer over a vertical flat plate. A laminar flow approximation is employed due to the small-length scales (< 5 cm), thereby reducing the burning crib to the classical description of the "Emmons problem" for forced-convection burning of a flat plate [44], shown schematically in Fig. 3. The framework of Emmons allows for a solution to the fuel-burning rate through a self-similarity solution of the momentum, energy, and species conservation equations. The mass transfer number B emerges as a boundary condition at the surface of the fuel, which can be modified to incorporate the physics of the crib and an external contribution from the compartment.

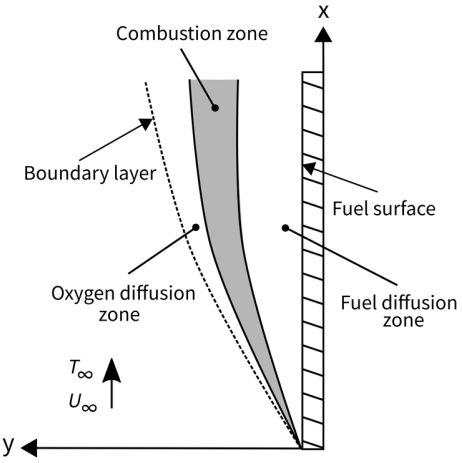

Figure 3: Formulation of the flat plate analogy for a stick burning inside a crib shaft

The classical Schvab-Zeldovich formulation necessary to derive the mass transfer number can be found in the literature [44], so only the necessary details are provided herein. Counterparts for natural convection can be found elsewhere [45–48]. By scaling the boundary layer conservation equations for a reacting flow and applying the flame sheet approximation, Emmons creates an analogy for momentum and energy transport that relates the heat transfer and shear stress at the fuel surface by

$$\dot{q}_0'' = -k\frac{\partial T}{\partial y}\Big|_{y=0} = \frac{c_{\mathrm{p},\infty}T_\infty(b_0 - b_\infty)}{u_\infty}\tau_0 \tag{8}$$

where $b_\infty - b_0 = \frac{1}{T_\infty c_{\mathrm{p},\infty}}\left(\Delta H_\mathrm{C} Y_{\mathrm{O}_2,\infty} + (h_\infty - h_0)\right)$ with ΔH_C corresponding to the heat of combustion per unit mass of oxygen, $Y_{\mathrm{O}_2,\infty}$ as the oxygen mass fraction, and h as the enthalpy of the flow in the free-stream (infinity subscript) and fuel surface (zero subscript) respectively. The shear stress at the fuel surface is given by $\tau_0 = \mu\left(\frac{\partial u}{\partial y}\right)\Big|_{y=0}$. It is assumed that the heat of combustion per unit mass of oxygen is ΔH_C = 13.1 kJ/g [49].

The surface heat flux is used to evaporate fuel and supply the heat losses, thus

$$\dot{q}_0'' = -(\Delta H_\mathrm{P} + Q)\dot{m}_\mathrm{b}'' \tag{9}$$

where ΔH_P is the heat of pyrolysis and Q is a general term for the heat losses at the surface per unit mass of fuel produced. By combining Eqs. (8-9), the burning rate of the fuel is related to the shear stress by a constant of proportionality B

$$\dot{m}''_{\mathrm{b}} = B\frac{\tau_0}{u_\infty} \tag{10}$$

with the mass transfer number B defined as

$$B = \frac{\Delta H_{\mathrm{C}} Y_{\mathrm{O}_2,\infty} - c_{\mathrm{p},\infty}\left(T_{\mathrm{ig}} - T_\infty\right)}{\Delta H_{\mathrm{P}} + Q} \tag{11}$$

The numerator of Eq. (11) is the total convective energy that is produced by combustion and is available to be conducted from the flame to the fuel to continue the pyrolysis process. The denominator corresponds to the energy requirements for pyrolysis and the heat losses, given as

$$Q = \frac{\dot{q}''_{\mathrm{L}}}{\dot{m}''_{\mathrm{b}}} \tag{12}$$

where $\dot{q}''_{\mathrm{L}}$ is an overall heat loss term that reflects all the energy that is driven away from the surface of the fuel and includes net radiative heat transfer, external heating, and in-depth conduction.

$$\dot{q}''_{\mathrm{L}} = \dot{q}''_{\mathrm{s,c}} + \dot{q}''_{\mathrm{s,r}} - \dot{q}''_{\mathrm{f}} - \dot{q}''_{\mathrm{e}} \tag{13}$$

Emmons assumes that the magnitude of $\dot{q}''_{\mathrm{L}}$ is sufficiently small such that the non-convective heat transfer terms only perturb convection and are therefore corrections to B. This allows for the boundary layer flow to be preserved. By approximating $\mathrm{Pr} = 1$, the energy-species equation is identical to the momentum equation, and the burning rate $\dot{m}''_{\mathrm{b}}$ can be obtained through by simply solving the Blasius equation, with B appearing as one of the boundary conditions at the fuel surface [44].

Acknowledging that the mass transfer number is formulated on the basis that the heat released by combustion is convective, Torero *et al*. [50] modifies Eq. (11) to correct for the radiation emitted to the environment, defining a total mass transfer number as

$$B_{\mathrm{T}} = \frac{(1-\chi)\Delta H_{\mathrm{C}} Y_{\mathrm{O}_2,\infty} - c_{\mathrm{p},\infty}\left(T_{\mathrm{ig}} - T_\infty\right)}{\Delta H_{\mathrm{P}} + Q} \tag{14}$$

where χ is the radiative fraction of the flames that depends on the flame emissivity.

The role of the crib geometry on the enhancement of B_{T} is evaluated by considering the pure convection case, where radiative losses from the flame can be neglected and heat losses and gains at the surface are balanced (i.e. $Q = 0$, $\chi = 0$). An adiabatic mass transfer number is then defined as

$$B_{\mathrm{A}} = \frac{\Delta H_{\mathrm{C}} Y_{\mathrm{O}_2,\infty} - c_{\mathrm{p},\infty}\left(T_{\mathrm{ig}} - T_{\infty}\right)}{\Delta H_{\mathrm{P}}} \tag{15}$$

The adiabatic mass transfer number B_{A} corresponds to Spalding's mass transfer number [51] and the first mass transfer number, B_{I}, from Eq. (4). B_{A} is a material property and assumes all the heat of combustion is used to increase the enthalpy of the flow and pyrolyze fuel. All other heat inputs cancel out. For well-ventilated stoichiometric combustion of softwood, $B_{\mathrm{A}} \approx 0.55$, assuming $c_{\mathrm{p},\infty} = 1$ kJ/kg K, $T_{\mathrm{ig}} = 568$ K, $T_{\infty} = 293$ K, $\Delta H_{\mathrm{P}} = 5$ kJ/g. The heat of pyrolysis taken for estimating B_{A} represents a nominal value that assumes no surface heat losses and was extracted from the analyses by Tewarson and Pion [52] and Quintiere and McCaffrey [11]. As $B_{\mathrm{A}} < 1$, the convective heat flux from the flame is insufficient to sustain combustion and the flame will quench. Therefore, the radiation conserved in-depth within the crib through $\dot{q}''_{\mathrm{b}}$ must be responsible for supplying the additional heat necessary to pyrolyze the fuel (i.e. $B_{\mathrm{T}} > 1$). Extinction does not follow as the pyrolysis is assisted by radiation [47,53] from the cross-radiating sticks. While the mass transfer number has been extended to incorporate absorption of external radiation in the flame [54], a solution to B_{T} must also consider the interaction of radiation on the flow field, which is not trivial to resolve [55] and can lead to a radiation-controlled regime of fires characterised by strong turbulent flows [56].

It has been postulated that when radiation increases, the similarity solution can break down as the radiation enhanced burning rate of the fuel can exceed the blow-off limit [44], therefore the flame geometry cannot be measured to quantify B_{T} due to the flow separation [50,53,57]. This is the case for very low airflow over a flat plate [58] and for turbulent boundary layers [56]. In the case of cribs, the enhancement of radiative exchange has a much more complex effect because it enhances char consumption (which enhances pyrolysis rates) as well as directly affecting the burning rate. Given the difficulties associated with this limit state, here, it will be assumed that the blow-off limit has not been attained.

Complications are not solely limited to the gas-phase as surface re-radiation and solid-phase conduction losses cannot be neglected and vary spatially along the streamwise coordinate [59–61]. For complex geometries like a crib, resolving the interaction of the flow fields and the heat transfer within the in-depth burning zone is not feasible. Therefore, an alternative approach to obtaining B_{T} for the free burning crib is necessary.

The approach to be followed will use some empirical observations to determine the crib free burning rate $\dot{m}''_{\mathrm{o}}$. This approach lumps the complex heat transfer terms in-depth within the crib, thus removing the need to quantify Q within the crib. Furthermore, radiative feedback from the compartment onto the crib surface, despite possibly being large, will be treated as a correction to the crib burning rate.

Experimental data for steady free burning of wooden slabs [62], cylinders [63], and high-porosity cribs [25,26,38] have shown that the steady-state burning rate of a charring solid is proportional to the thickness b of the solid by $\dot{m}''_{\mathrm{o}} \propto b^{-0.5}$. Block proposed the following expression that defines the burning rate of a well-ventilated crib in terms of the dimensions of a single stick

$$\dot{m}''_{\mathrm{o}} = C b^{-0.5} \tag{16}$$

where C is an empirically-determined constant of proportionality that serves to quantify the total heat transfer. Block considers this constant independent of geometry and therefore is a property of the solid and the fluid. Eq. (16) is only valid if the crib porosity factor satisfies the open-regime provided that the porosity is not so large that $\dot{q}''_{\mathrm{b}}$ is insufficient to sustain continuous combustion of the crib.

While Eq. (16) might include radiation feedback from the flame, radiation-dominated burning requires additional energy input that is provided by the constant "C". The mass flux generated by the incident radiation on the surface is described by Eq. (7) and will be added as a correction to the crib burning rate to formulate the total burning rate

$$\dot{m}''_{\mathrm{b}} = \dot{m}''_{\mathrm{o}} + \dot{m}''_{\mathrm{r}} = \frac{\dot{m}_{\mathrm{o}}}{A_{\mathrm{s}}} + \frac{\dot{m}_{\mathrm{r}}}{A_{\mathrm{s,t}}} \tag{17}$$

Considering the projection of the burning crib over a floor area, the surface areas can be defined using geometrical ratios

$$A_{\mathrm{s}} = R_1 L_{\mathrm{P}} W \tag{18}$$

$$A_{\mathrm{s,t}} = R_2 L_{\mathrm{P}} W \tag{19}$$

where R_1 and R_2 is the ratio of the exposed surface areas to floor area [19], L_{P} is the surface pyrolysis length defined as the distance from the flame front to the burnout front, and W is the width of the fuel-bed. It is assumed that the flame and burnout fronts are uniform across the width of the fuel and spread is one-dimensional. For simplicity, the ratio of the surface areas can be expressed in terms of A_{s} leading to

$$\frac{A_{\mathrm{s,t}}}{A_{\mathrm{s}}} = \frac{R_2}{R_1} = \psi \tag{20}$$

Combining Eqs. (7), (16) and (17) with Eqs. (18 to 20), the total crib burning rate is

$$\dot{m}''_{\mathrm{b}} = C b^{-n} + \frac{1}{\Delta H_{\mathrm{P}}} \psi \dot{q}''_{\mathrm{e}} \tag{21}$$

The evaluation of the individual heat losses (Eq. (13)) within the numerator of the overall heat loss term $Q = \dot{q}''_{\mathrm{L}} / \dot{m}''_{\mathrm{b}}$ is a complex endeavour, therefore the term will be approximated as a fraction of the external input defined by the ratio of areas ($\dot{q}''_{\mathrm{L}} = -\psi \dot{q}''_{\mathrm{e}}$). Therefore, thermal feedback from the compartment is treated as a heat input and this simple expression substitutes Eq. (13). By substituting the new definition of $\dot{q}''_{\mathrm{L}}$ and Eq. (21) into Eq. (12), an expression for the heat loss term Q that appears in the dominator of the mass transfer number (Eq. (14)) is found

$$Q = \frac{-\psi \dot{q}''_{\mathrm{e}}}{C b^{-n} + \frac{1}{\Delta H_{\mathrm{P}}} \psi \dot{q}''_{\mathrm{e}}} \tag{22}$$

It is important to note that this simple substitution is possible because once the energy enters the crib, it will be retained in-depth, and whatever form of heat transfer is involved (as per Eq. (13)) it will not change the net input. The formulation of Q imposes a condition that the primary external driver of heat transfer is by radiation, nevertheless the mechanism by which heat transfer (in-depth) delivers the total burning rate will change with $\dot{q}''_{\mathrm{e}}$.

A total mass transfer number, B_{T} for a wood crib can be then established by combining Eq. (14) with Eq. (22)

$$B_{\mathrm{T}} = \frac{\left(Cb^{-n} + \frac{1}{\Delta H_{\mathrm{P}}}\psi\dot{q}''_{\mathrm{e}}\right)\left[(1-\chi)\Delta H_{\mathrm{C}}Y_{\mathrm{O_2},\infty} - c_{\mathrm{p},\infty}\left(T_{\mathrm{ig}} - T_{\infty}\right)\right]}{\Delta H_{\mathrm{P}}\left(Cb^{-n} + \frac{1}{\Delta H_{\mathrm{P}}}\psi\dot{q}''_{\mathrm{e}}\right) - \psi\dot{q}''_{\mathrm{e}}} \tag{23}$$

The total mass transfer number B_{T} for a crib (Eq. (23)) carries one independent variable, the external heat flux from the compartment ($\dot{q}''_{\mathrm{e}}$). The remaining terms are properties of the solid and fluid and are obtained either from the literature or are geometrical properties of the crib. The formulation of Eq. (23) supposes that the crib is well-ventilated and burns at stoichiometric conditions with infinite chemistry, thus the burning rate is based on thermal considerations. Flames external to the crib are assumed as optically-thin, therefore radiation from the flames can be greatly simplified by treating χ as a constant and neglecting $\dot{q}''_{\mathrm{f}}$ in the definition of Q. The total mass transfer number corresponds to the free burning crib when $\dot{q}''_{\mathrm{e}}$ = 0.

3. Experimental description

The full description of the experimental set-up and results of the Malveira Fire Test are detailed by Hidalgo *et al.* [18], however, a brief overview of the relevant characteristics of the test are provided. The internal compartment dimensions measure 4.7 m (depth), 21.0 m (length), and 2.85 m (height). Five opening windows of varying dimensions are located along the front wall of the compartment. The internal lining material consists of a masonry block infill with a notable exception; a combustible cork insulation covering approximately 60% of the ceiling. A schematic of the compartment and fuel placement is presented in Fig. 4. The cork insulation is located on the right-hand side of the compartment after a protruding soffit (identified by the dark shading). The inverse opening factor (ϕ') is 4.6 $\mathrm{m}^{-0.5}$ corresponding to a well-ventilated compartment in the framework by Thomas and Heselden [6].

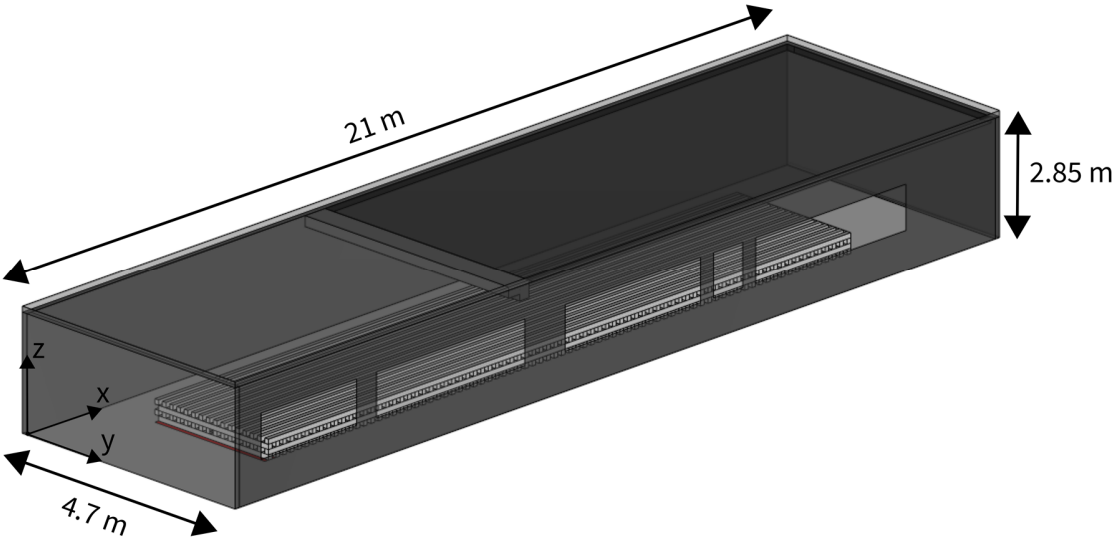

Figure 4: Experimental set-up for the Malveira Fire Test.

The fuel-bed consisted of a continuous wood crib of Pinus Pinaster sticks, consisting of 14 individual cribs combined that measured 16.8 m long x 2.4 m wide. The crib is comprised of three full layers and one-half layer of sticks, with the top layer of sticks aligned parallel to the direction of flame spread. Each stick measures 1.2 m long with a 5 cm x 5 cm square cross-section. Ignition of the crib is attained using a mixture of 5 L of kerosene and 0.5 L of diesel fuel placed in 2.4 m long x 10 cm x wide x 5 cm high metal tray that is positioned at the start of the crib in place of two of the lowest sticks. The crib is ignited along the start of the fuel bed on the left-hand side of the compartment. In the full layers, the sticks were evenly spaced at 5 cm, thus the cross-sectional area of each vertical shaft is uniform, and the crib porosity calculated using Eq. (2) is 0.25 cm; corresponding to the open-regime [9]. The total exposed surface area of wood to air (A_S) is approximately 228 m² [19]. Three moisture content measurements were taken per crib, with an average moisture content of 19% ± 6% [18]. The individual moisture content for each crib is shown in Fig. 5.

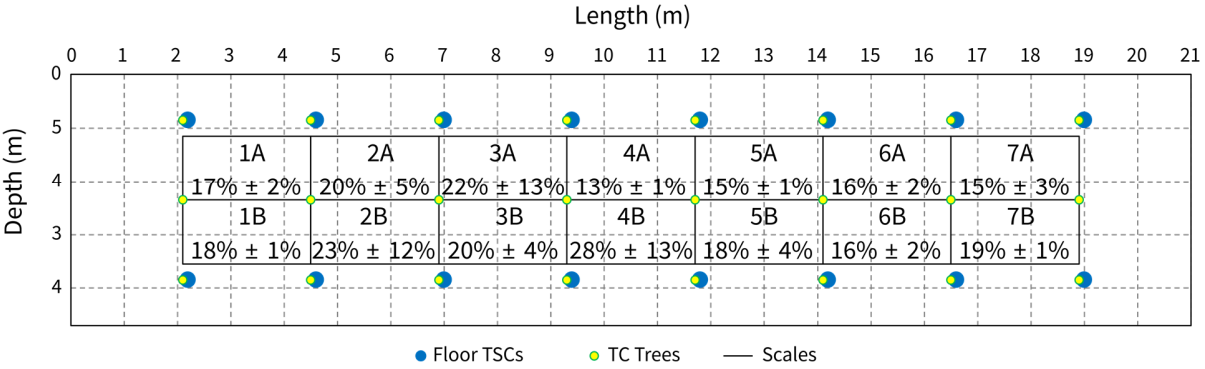

Figure 5: Plan diagram of the internal dimensions and instrumentation layout of the floor. The platforms for each mass loss scale (1A – 7B) are shown with the measured moisture contents for each crib.

Each crib was loaded onto a bespoke platform system that was supported by a mass loss scale and arranged continuously to capture the entire crib mass loss rate (MLR) [18]. The mass loss scales were calibrated and levelled onsite by Levantina de Pesaje (manufacturers), with an accuracy of 20 g. Contact between the platforms was minimised as far as reasonably practicable.

Thin-skin calorimeters (TSCs) were used to quantify the incident radiant heat flux to the fuel ($\dot{q}''_e$). A total of 16 TSCs were mounted into the floor of the compartment, with 8 TSCs located adjacent to the fuel-bed on each side, as shown in Fig. 5. The design and calibration of the TSCs follow the methodology provided by Hidalgo *et al*. [64]. Five network cameras were positioned at each window to capture the position of the flame front and burnout front along the length of the compartment. These cameras were mounted on a cantilevered beam approximately 2 m out from the corresponding window sill. The cameras only captured the flame and burnout front positions on the surface of the crib [18].

4 Results

4.1 Experimental Results

Image analysis of video recordings of the Malveira Fire Test was applied by Gupta *et al*. [19] to obtain the time evolution of the surface flame front (x_{FF}) and burnout front positions (x_{BO}). Assuming a line fire across the width of the fuel-bed, a surface pyrolysis length is defined by the difference between the measured positions of the surface flame front and the burnout front at each time-step ($L_P(t) = x_{FF}(t) - x_{BO}(t)$). The position of the surface flame front and the burnout front along with the calculated pyrolysis length is shown in Fig. 6a. The instantaneous velocity of the surface flame ($V_{S,sf}$) and burnout (V_{BO}) fronts are shown in Fig. 6b and were also obtained from Gupta *et al*. [19] using a second-order central differencing scheme for the first derivative of the measured front positions.

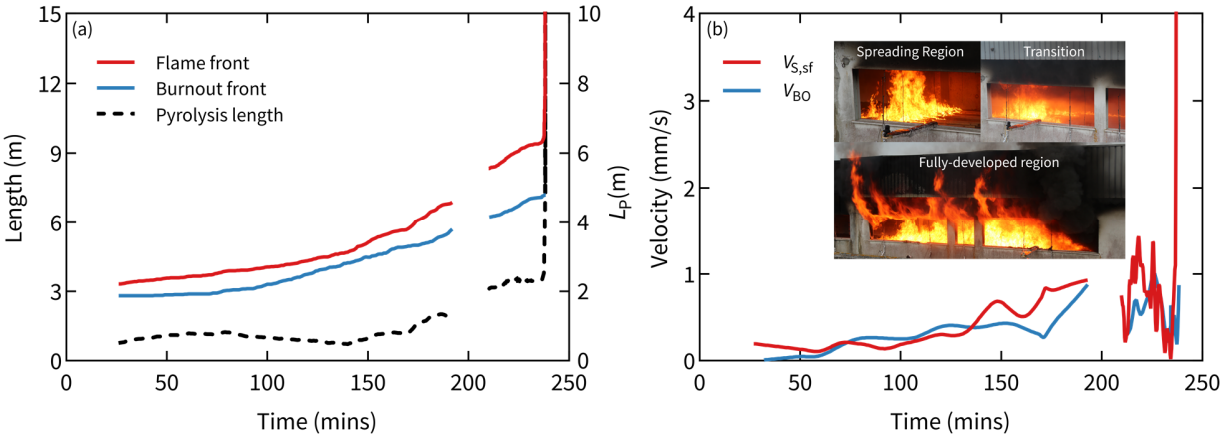

Figure 6: (a) Position of the flame and burnout fronts obtained using image processing analysis from the video footage from the cameras at the window. The pyrolysis length is calculated as the difference of the two fronts assuming that the fire is uniform along the width of the crib. (b) Instantaneous velocities of the flame and burnout fronts over the evolution of the fire. The data for this test has been obtained from Gupta et al. [19].

Based on the ratio of the instantaneous propagation data of the fire ($V_{S,sf}/V_{BO}$), the evolution of the fire can be segmented into two distinct regions. The first region corresponds to a travelling fire ($V_{S,sf}/V_{BO} \approx 1$) from 26 mins to 107 mins. The fire accelerates slowly in the second region corresponding to a growing fire ($V_{S,sf}/V_{BO} > 1$) and lasts from 107 mins to 237 mins. At approximately 235 mins, the cork ceiling ignites and flames start to spread along the ceiling. The flaming ceiling and descending smoke layer increases the thermal feedback, $\dot{q}''_e$ onto the unburned surface of the crib, accelerating the surface spread rate [19]. At approximately 237 mins, flames

rapidly spread across the remaining unburned surface of the crib. Shortly afterwards, the in-depth burning zone also spreads to the end of the crib. The instance that the in-depth and surface burning zones equate defines a fully-developed fire that burns until 241 mins when the fire is manually extinguished. Here, we will analyse the periods under which the flame front is spreading (i.e. the travelling fire, $V_{S,sf}/V_{BO} \approx 1$ and growing fire, $V_{S,sf}/V_{BO} > 1$ modes from 26 – 237 mins) and the transition to a fully-developed fire ($V_{S,sf}/V_{BO} \to \infty$ from 237 to 241 mins) independently.

4.2 Spreading region

Time-resolved experimental burning rates are obtained with measurements of the mass loss rates and area of the surface burning zone by

$$\dot{m}''_b(t) = \frac{\dot{m}_b(t)}{R_1 L_p(t) W} \tag{24}$$

Mass loss rates are obtained using the load cell data from Hidalgo *et al*. [18] and the area of the burning zone is calculated using the defined pyrolysis length under the assumption that the flame front is constant across the width of the fuel bed. Measurements of $\dot{q}''_e$ are extracted from the TSCs following [64] and the heat fluxes at the flame and burnout fronts are obtained from Gupta *et al*. [19]. The experimental heat flux from the compartment that is applied over the pyrolysis length is given as

$$\dot{q}''_e(t) = \frac{1}{L_P} \int_{x_{BO}}^{x_{FF}} \dot{q}''_e(x)\, dx \tag{25}$$

where x_{FF} and x_{BO} corresponds to the flame front and burnout front positions respectively.

Figure 7 shows the time-evolution of the experimental burning rate for the spreading fire region of the experiment. A critical mass flux, $\dot{m}''_{cr}$, for flaming extinction of softwood is shown for reference. This value was obtained under bench-scale testing conditions of timber blocks and generally ranges within 3.5 to 4.0 g/m^{-2}.s^{-1} [65–67] across different species of wood and experimental apparatus. Thus, $\dot{m}''_{cr}$ is a useful reference to highlight non-physical values from the experimental data.

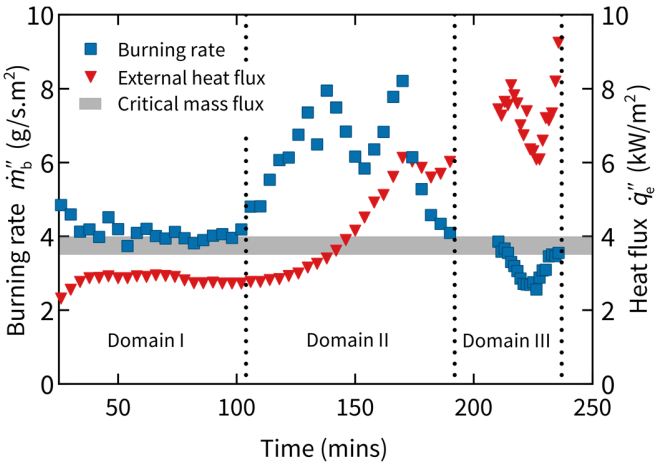

Figure 7: Time evolution of the experimental burning rate (Eq. (24)) and heat flux (Eq. (25)) during the spreading region of the Malveira Fire Test.

Three distinct trends in the burning rate are identified in Fig. 7. These are separated into distinct time domains. Average burning rates for each time domain are 4.24 g/m^{-2}.s^{-1}, 6.19 g/s^{-1}.m^{-2} and 3.25 g/s^{-1}.m^{-2}. Variations in the measured burning rates are not synchronous with the measured heat fluxes in the compartment and are likely attributed to errors in the estimated pyrolysis lengths over certain time domains. This is particularly the case in Domain III, which falls below $\dot{m}''_{cr}$, and is therefore unphysical. These errors are associated with the breakdown of the line fire assumption as the fire starts spreading faster, thus incorrect flame positions are measured, leading to incorrect calculation of the burning rate. From Eq. (24), it can be expected that $\dot{m}''_b(t) \sim L_p$ by some constant of proportionality. To help identify the breakdown in the line fire assumption, the burning rate and the pyrolysis length in each time domain are normalised by their maximum values and are compared to each other in Fig. 8.

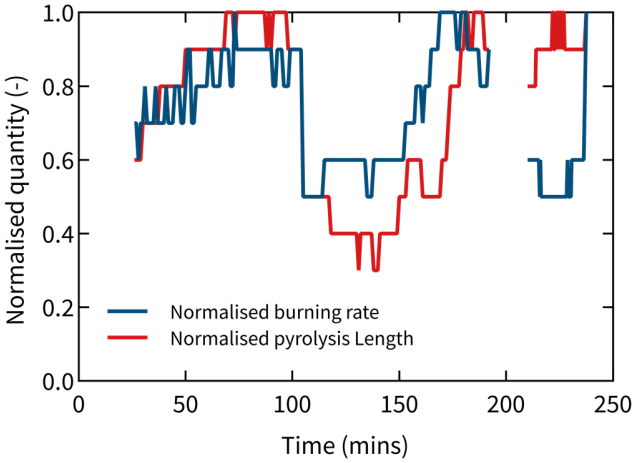

Figure 8: Correlation of the normalised burning rate and the pyrolysis length for each time domain during the spreading region of the Malveira Fire Test.

In Domain I, the normalised burning rate and pyrolysis length correlate well, demonstrating that the surface burning zone corresponds to the in-depth burning zone (i.e. the flame front is uniform in-depth within the crib). This trend starts to diverge in Domain II and completely diverges in Domain III. The divergence of the normalised pyrolysis length and burning rates in Domain III confirms that the error in defining $\dot{m}''_b$ originates from two sources: (1) the surface burning zone does not correspond to the in-depth burning zone, and (2) the line fire assumption across the width of the crib does not hold. The in-depth burning zone cannot be identified from the camera footage. The supplementary figure in Appendix S1 shows the variation of the MLR across the width of the crib for the scales during the spreading region of the fire. Deviations in the measured MLR across the width of the fuel bed range from 15 to 25 g/s. The spatial distribution is likely associated to larger heat fluxes towards the back wall of the compartment and variations in the crib moisture content. Domain III is excluded from the analysis of the mass transfer number due to the significant errors in estimating the burning zone.

4.3 Fully-developed region

Once rapid flame spread occurs after 237 mins, the remaining fuel becomes involved in the fire. The timescales for the entire crib to become involved is short, approximately lasting 1 to 1.5 mins and can be observed by the attainment of steady mass loss rates for the remaining scales. The data for the mass loss scales during this region are shown on the supplementary figure in Appendix S2. This type of fire is referred to in the literature as fully-developed or a post-flashover fire. The large openings ventilate the compartment, and therefore the measured thermal fields in the fully-developed region are heterogeneous [18], a characteristic that is consistent with fuel-controlled

compartment fires [13]. To evaluate the burning rate of the crib spatially, measured values for $\dot{m}_b''$ and $\dot{q}_e''$ are discretised by each of mass loss scales. The external heat flux associated with each mass loss scale are obtained by averaging measured values of $\dot{q}_e''$ from the TSCs adjacent to each scale. The spatial evolution of $\dot{m}_b''$ and $\dot{q}_e''$ along the length of the fuel-bed are shown on Fig. 9 for the crib located (a) towards the opening (2.4 m ≤ y ≤ 3.6 m), and (b) towards the back wall (1.2 m ≤ y ≤ 2.4 m). The data is averaged for each scale from the instance that the MLR initially spikes on each scale to the point of suppression.

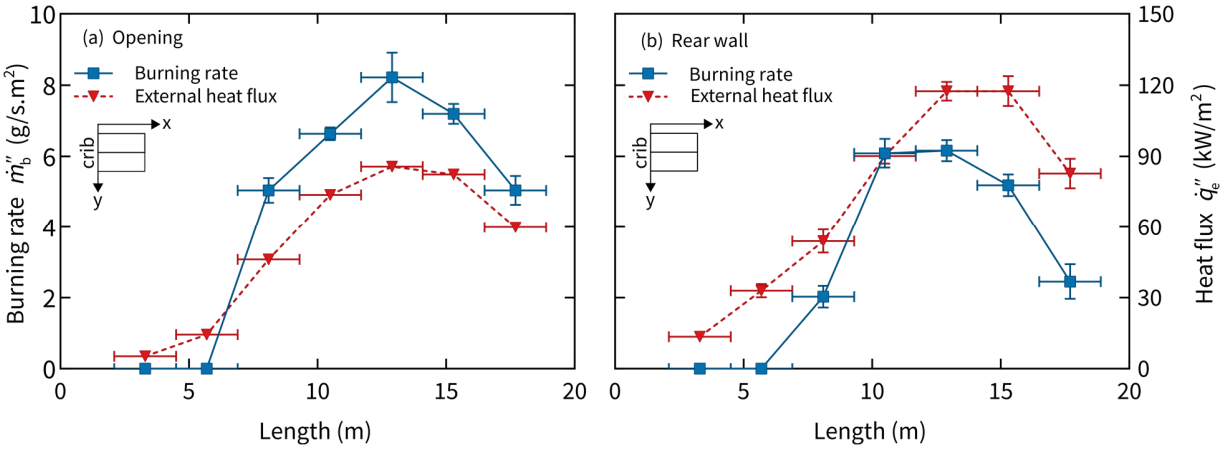

Figure 9: Spatial variation of the burning rates and heat fluxes for the fully-developed crib fire.

The error bars in Fig. 9 show the 95% confidence interval for the measured burning rates and heat fluxes. The data clearly shows that the burning region is localised within 6.9 m and 18.9 m. Video footage of the fully-developed fire shows "flame necking" behaviour due to lateral entrainment, leading to lower burning rates and heat fluxes towards the edges of the surface and in-depth burning zones. Contrasting the burning rates and heat fluxes across the width of the fuel-bed shows that burning rates are larger towards the opening despite significantly lower measured values of $\dot{q}_e''$. This characteristic is a departure from the burning dynamics observed when the fire was spreading and indicates that the burning rate is controlled by the capacity of oxygen to be entrained into the fire and in-depth within the crib. The reduction in the burning rate towards the back wall is likely associated to a reduction in the oxygen mass fraction within the crib as the oxygen entrained into the compartment is consumed at the crib surface towards the opening. Consequently, the high porosity factor of the crib has little influence on the burning dynamics as the residence times are too short to allow oxygen to diffuse into the porous media, and therefore the crib is not well-ventilated. Larger heat fluxes towards the back wall are indicative of momentum-driven flows as the fire acts as a pump and is tilted by the inflow air. The non-uniform nature of the flame shape leads to a radiative fraction χ and flame heat flux $\dot{q}_f''$ that is ill-defined. The large spatial distribution of burning rates demonstrates that conditions external to the crib such as the thermal feedback, oxygen concentration, radiative fraction and flame emissivity are competing parameters that control the burning rate and evolve significantly in space. These parameters are not trivial to quantify and are dependent on the interaction of the fuel-bed with the flow fields.

5 Discussion

The role of the crib structure and thermal feedback from the compartment on the burning dynamics of the crib can be evaluated by contrasting the theoretical modified mass transfer number B_T defined by Eq. (23) to experimentally obtained values of B_T. In both cases, B_T will be evaluated as a

function of $\dot{q}_e''$ to explicitly identify the controlling processes delivering the crib burning rate within the compartment. External radiation is assumed to be delivered solely from the smoke layer and compartment boundaries by approximating the flame as optically-thin. These assumptions are consistent with the definition of the processes governing the in-depth burning and flame spread of the crib.

The crib constant C can be obtained from Eq. (16) towards the free burning limit, $\dot{q}_e'' \to 0$ (i.e. early in the test before a strong smoke layer contribution is established). To simplify the analysis, a single value for C is extracted by averaging the experimental values for $\dot{m}_b''$ in Domain I, yielding $C \approx 0.94$ mg/s cm$^{1.5}$. This approximation is consistent with values found by Block for softwoods (0.86 – 1.11 mg/s cm$^{1.5}$) [38]. Taking χ = 0.21 [41], ΔH_c = 13.1kJ/g, $Y_{O_{2,\infty}}$ = 0.233 and $c_{p,\infty}$ = 1 kJ/kg K for the gas-phase properties, and by taking T_{ig} = 568K [19], T_∞ = 293K, ψ = 0.12 [19], b = 5 cm, n = 0.5 [38] and ΔH_P = 1.8 kJ/g [11] as the fuel properties, B_T is theoretically evaluated. It is worth noting that ΔH_P is defined using an effective value measured from experiments that are inclusive of surface losses.

By substituting the terms comprising the theoretical burning rate in Eq. (23) for an experimental burning rate ($\dot{m}_b''(t)$), an experimental mass transfer number that evolves in time can be formulated using the data obtained for the burning rate (Eq. 24) and the heat flux (Eq. 25)

$$B_T(t) = \frac{\dot{m}_b''(t)\left[(1-\chi)\Delta H_C Y_{O_{2,\infty}} - c_{p,\infty}\left(T_{ig} - T_\infty\right)\right]}{\Delta H_P \dot{m}_b''(t) - \psi \dot{q}_e''(t)} \tag{26}$$

where the temporal variation in the heat transfer is explicitly defined within Q. The experimental burning rate, $\dot{m}_b''(t)$ and heat flux, $\dot{q}_e''(t)$ are extracted from Fig. 7 and Fig. 9 for both regions of the Malveira Fire Test. Using this approach, the experimental value of $B_T(t)$ can be evaluated with the corresponding measured heat flux $\dot{q}_e''(t)$ and is contrasted to the theoretical mass transfer number from Eq. (23) as shown in Fig. 10.

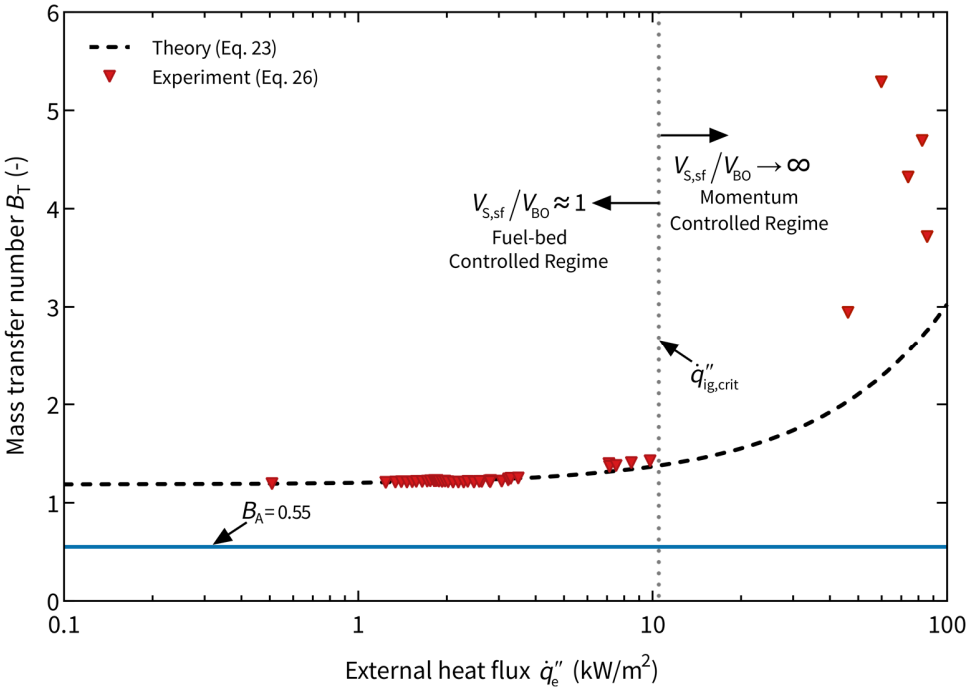

Figure 10: Theoretical (Eq. (23)) and experimental (Eq. (26)) total mass transfer numbers plotted as a function of the external heat flux from the compartment.

Two regimes of burning behaviour are identifiable from Fig. 10, which shows the variation of experimental and theoretical values of the crib mass transfer number B_T as a function of $\dot{q}''_e$. The vertical dotted line indicates the transition point and corresponds to the critical heat flux for ignition of the fuel, $\dot{q}''_{ig,crit}$ [19], which demarcates the two identified regimes. Once the thermal feedback from the compartment exceeds this value, a highly transient rapid flame spread takes place leading to a fully-developed fire [19]. Below $\dot{q}''_{ig,crit}$, the fire is characterised by $V_{S,sf}/V_{BO} \approx 1$ corresponding to the spreading region of the fire. Above this critical value, the fire can be characterised as fully-developed ($V_{S,sf}/V_{BO} \to \infty$) with very large heat fluxes. The adiabatic mass transfer number B_A for softwood as calculated earlier is shown (horizontal line) to demonstrate the effect of radiation heat transfer in-depth within the crib. Data from Domain III in the spreading region (Fig. 7) and the mass loss scales towards the back wall in the fully-developed region (Fig. 9b) are excluded from the analysis. In the former case, the flame length and $\dot{m}''_b$ is ill-defined, and in the latter case, the data indicates that crib is starved of oxygen and B_T cannot be calculated as the oxygen mass fraction is not known within the crib. The proceeding sections will discuss the characteristics of each regime and the transition from one regime to another.

5.1 Burning regimes

Towards the limit for a free burning crib ($\dot{q}''_e \to 0$), the mass transfer number of the crib is extracted as $B_T = 1.19$ and when normalised by adiabatic mass transfer number, $B_T/B_A = 2.16$. The large ratio of B_T/B_A indicates that radiation in-depth within the crib is the driving force for the burning dynamics and in-depth flame spread under conditions of no external heating as the convective heat flux from the flame is too weak to enable surface flame spread. The data shows that B_T is insensitive to changes in $\dot{q}''_e$ at heat fluxes below $\dot{q}''_{ig,crit}$. The good fit of the data to the theory in this region

demonstrates that the crib burns under stoichiometric conditions, and is therefore well-ventilated, with an optically-thin flame established over the crib. The porous nature of the fuel-bed insulates the fuel from external effects, and therefore the crib itself acts as a fire source that defines the compartment fire dynamics. The limit for this behaviour defines a fuel-bed-controlled regime where the in-depth and surface flame front velocities are in equilibrium with the burnout front velocity ($V_{\mathrm{S,id}} \equiv V_{\mathrm{S,sf}} \equiv V_{\mathrm{BO}}$), the magnitude of which is quantified by the geometry and physical properties of the wood crib. Consequently, this regime corresponds to a travelling fire spread mode ($V_{\mathrm{S,sf}}/V_{\mathrm{BO}} \approx 1$) for wood crib fires.

The fully-developed region is characterised by large external heat fluxes ($\dot{q}''_{\mathrm{e}} > 70$ kW/m^2) that significantly enhance the crib burning rate and the total mass transfer number B_{T}. The scatter in B_{T} is large and shows that the momentum-driven flow field above the crib has a controlling effect on the crib burning rate. The theory in this region underpredicts the data and is associated with an incorrect formulation of the crib burning rate (Eq. 21), which assumes that the crib is well-ventilated and burns stoichiometrically. Instead, the crib burns fuel-rich as the porous media is no longer insulated from external processes. The crib burning rate is controlled by oxygen transport into the crib; a characteristic of the spatiotemporal evolution in the flow field. Due to the reduction in the free crib burning rate, radiative-driven burning over the surface of the crib ($\dot{m}''_{\mathrm{r}}$) is the driving force for energy production in the compartment. The flames occupy a large area, therefore the approximation of an optically-thin flame is not valid, leading to an ill-defined heat loss term, Q and radiative fraction, χ. Thermal feedback from the compartment and flames are spatially distributed as the inertia of the flow heavily influences local flame geometry. Unburned pyrolyzates generated near the openings are transported and burned towards the back wall. The analysis shows that at the large limit of heat fluxes, the burning dynamics are governed by the flow residence time. Burning rates are a local quantity that is defined by non-uniform transport processes external to the crib, thereby defining a momentum-controlled regime. In this regime, oxygen transport into the porous fuel is limited by the complex interaction of the flows induced by the compartment geometry, flame geometry, thermal feedback, and fuel-bed structure. This burning regime corresponds to the fully-developed fire spread mode ($V_{\mathrm{S,sf}}/V_{\mathrm{BO}} \to \infty$).

5.2 Transition of regimes

Transitions from the fuel-bed-controlled regime to the momentum-controlled regime are induced by raising the solid temperature T_{s} towards an ignition temperature T_{ig} by the arrival of the flame front such that $V_{\mathrm{S,sf}} \gg V_{\mathrm{S,id}}$. The increased energy input into the compartment from the surface burning zone leads to two conditions: (1) an increase in the external heat flux due to the heating of the smoke layer, and (2) contribution of the feedback from the flame heat flux is established as the flame transitions to optically-thick. These two factors induce the fast flame spread of the crib in-depth that formalises the transition to a fully-developed fire spread mode. The delay time to attain peak measured MLRs is very short at approximately 45 seconds for the remaining cribs (Appendix S2), therefore in-depth flame spread rate asymptotes to infinity at this point.

These results are consistent with Thomas' theory that thermal feedback from the flames ($\dot{q}''_{\mathrm{f}}$) above the crib can no longer be ignored from the energy equation in Eq. (6) at a particular length-scale, thereby inducing "fast spread". The characteristic timescales associated with the transition to a fully-developed fire with the entire crib in-depth burning once rapid flame spread of the surface occurs ($V_{\mathrm{S,sf}} \to \infty$) is relatively short as the additional energy input from the flames and compartment induces rapid flame spread within the crib in-depth ($V_{\mathrm{S,id}} \to \infty$). Due to the short timescales associated with this transition, the crib burning dynamics can be described in terms of

the two steady-state regimes. The transition of regimes is ultimately a surface spread problem, that can be defined by a critical heat flux for rapid spread $\dot{q}''_{\mathrm{rs,crit}}$, a quantity that is bounded by the critical heat flux for ignition $\dot{q}''_{\mathrm{ig,crit}}$ under steady-state testing conditions [19].

5.3 Implications for large mass transfer number fuels

A natural question arises regarding the applicability of the analysis presented herein on wood cribs to the burning of large mass transfer number fuels that lay above unity such as non-charring plastics in compartments. The adiabatic mass transfer number B_{A} of non-charring plastics lies above unity, therefore the fuel pyrolyzes considerably faster than cellulosic fuels [52]. The absence of an oxidising char layer reduces the solid-phase losses and therefore allows more heat to pyrolyze fuel leading to larger burning rates. It is also important to note that influence of the fuel structure in defining the total mass transfer number B_{T}. It has been shown that the crib structure insulates the burning wood within the porous media from external heating by the flames and compartment above the crib unless the fire is very large. Pyrolysis rates of the wood within the crib rely on the radiation received from other sticks and the heat produced by the oxidation on the surface of the char layer. It is for this reason that charring plastics such as polyurethane in crib configurations burn analogous to wood cribs [10,11]. The absence of an oxidising char layer in non-charring materials reduces the emissivity of the burning zone. Pyrolysis of the fuel within the crib structure must therefore rely on the heat produced by a combination of re-radiation from the non-charring sticks, the energy released by combustion within the vertical shafts and the thermal feedback from the flames and compartment. Under free burning conditions ($\dot{q}''_{\mathrm{e}} = 0$), it is difficult to speculate as to the exact mechanisms driving the burning rate for cribs comprised of non-charring plastics due to the very limited quantity of experimental data, which offers conflicting results to the relation of the exposed surface area of the crib (by increasing the crib height) to the burning rate for small cribs [10,68,69]. The experiments by Harmathy for polylite (PLA) shows that increasing the crib height reduces the burning rate [68], suggesting that the flames above the crib control the burning rate, whilst the experiments by Yung for polymethylacrylic (PMMA) show the opposite, suggesting that processes inside the crib control the burning rate [69]. Nonetheless, burning rates are expected to still be larger for cribs consisting of non-charring fuels due to the large adiabatic mass transfer number B_{A}. Furthermore, enhancement of the burning rate by external radiation for non-charring fuels over the exposed surface area on top of the crib will be more profound due to the lower heat losses.

Non-charring plastics carry a stoichiometric air requirement that is two to three times greater than cellulosic fuels. For large compartments where oxygen inflow is not restricted by the openings, an increased burning rate will accelerate the flows within the compartment as the air is entrained into the flame envelope along the ceiling and through the openings. The efficiency of air entrainment into the flame envelope inside the compartment controls the thermal feedback onto the fuel and is dependent on the fire spread mode ($V_{\mathrm{S,sf}}/V_{\mathrm{BO}}$) and the compartment geometry, both of which defines the flow fields. Burning fuels with large mass transfer numbers such as PMMA and PE in configurations such as cribs, pools, or solid slabs in fully-developed compartment fires at small-scale geometries have shown that while the burning rates are considerably enhanced by thermal feedback, significant quantities of pyrolyzates burn outside the compartment. In these experiments, the flame envelope extends significantly through the opening [68,70,71] as the airflow into the compartment is reduced once quasi-steady conditions are attained. The consequence of this are lower temperatures inside the compartment, and therefore a reduction in the thermal feedback onto the fuel when compared to wood cribs [71,72]. It should be emphasised that these experiments were all conducted in small cubic compartments with small openings and are not comparable to large compartments as the quantity of pyrolyzates burned within the compartment

is geometry dependent. Furthermore, due to the strong coupling of the burning rate and thermal feedback for non-charring fuels irrespective of the fuel-structure [68,70–72], the burnout front velocity V_{BO} can not be regarded as a constant that is solely dependent on the crib geometry and mass per unit area of fuel. It would be expected that V_{BO} will evolve in time during the progression of the fire as the compartment heats up. Moreover, the surface flame spread rate $V_{\mathrm{S,sf}}$, a parameter that is associated with the thermal inertia ($k_{\mathrm{s}}\rho_{\mathrm{s}}c_{\mathrm{s}}$) and the ignition temperature (T_{ig}) of the fuel, is also controlled by the external heat flux from the compartment which also evolves in time. Therefore, the fire spread mode ($V_{\mathrm{S,sf}}/V_{\mathrm{BO}}$) for non-charring fuels depends on the competing timescales of spread and burnout [19], both of which will evolve in time and are heavily dependent on the thermal feedback that is strongly related to the compartment geometry.

In the absence of data on spreading or fully-developed fires involving non-charring fuels in large compartments, any commentary is speculative. However, the analysis presented herein on wood cribs has shown that the charring nature of the fuel-bed is fundamental in insulating the porous media from the external effects of the compartment and therefore has a very mild effect on V_{BO}. Non-charring fuels with large mass transfer numbers are more sensitive to thermal feedback, and thus the burning rate evolution is dependent on the fuel structure and the compartment geometry. The spatial and temporal evolution of the burning rate for large mass transfer number fuels is strongly related to the interaction of the flow fields induced by compartment geometry with the fuel geometry and cannot be resolved presently. Extrapolation of existing theories and models derived from compartment fire experiments using wood cribs to non-charring fuels or fuel arrangements other than cribs is therefore untenable and must be done with extreme caution.

6 Conclusions

This work studies the heat and mass transport processes defining the burning dynamics and in-depth flame spread of wood crib fires in large compartments. A theory that describes the process in-depth and external to the crib is presented. The coupling of these processes is studied by analogising the burning wood crib to the description of the “Emmons problem”, thereby enabling the formulation of a total mass transfer number B_{T}. Heat and mass transfer processes in-depth within the crib are simplified using an empirical formulation for stoichiometric burning of a crib and incorporated into B_{T}. External radiation from the compartment is treated as a correction to B_{T} that enhances burning over the crib surface. The theory is compared to data collected from a large-scale compartment fire test. Comparisons of the data to the theory show two steady-state regimes that define the burning dynamics of the crib: a fuel-bed-controlled regime and a momentum-controlled regime.

The fuel-bed-controlled regime occurs towards the small external heat flux limit. In this regime, B_{T} is insensitive to external radiation from the compartment. In-depth and surface flame spread rates are in equilibrium with the burnout front velocity, with the magnitude determined by the crib porosity and geometry. The wood crib is insulated from external effects and burns within stoichiometric ranges. Therefore, the wood crib acts as a fire source that defines the compartment fire dynamics. The momentum-controlled regime corresponds to the fully-developed fire at the large heat flux limit. In this regime, B_{T} is significantly enhanced by external radiation and varies locally across the burning fuel-bed. Burning is no longer stoichiometric, and the total burning rate is controlled by the residence time, with the momentum-driven flows heavily influencing the air entrainment and flame geometry. Transitions from the fuel-bed-controlled regime to the momentum-controlled are initiated once the thermal feedback is sufficiently large enough to induce rapid flame spread across the surface of the crib. The additional energy input mechanism from the

now optically-thick flames and compartment into the porous media significantly increases the flame spread rate in-depth within the wood crib, and therefore a transition to the momentum-controlled regime is short. The regimes and processes identified for wood cribs are not compatible with non-charring fuels with adiabatic transfer numbers above unity as the burning mechanisms diverge to that of wood cribs. Extreme caution should be exercised when extrapolating the test data of wood crib fires in compartments to non-charring fuels or fuel arrangements other than cribs.

Acknowledgements

This work forms part of the Real Fires for the Safe Design of Tall Buildings Project funded by the EPSRC (Grant No. EP/J001937/1) at The University of Edinburgh. The authors are grateful to the EPSRC for funding this work. The authors are indebted to the experimental team and supporting partners responsible for the generation of the data from the Malveira Fire Test and are grateful to Tristan Goode for early work analysing the raw data from the test.

References

[1] P.H. Thomas, Behavior of fires in enclosures-Some recent progress, Symp. (Int.) Combust. 14 (1973) 1007–1020.

[2] J.L. Torero, A.H. Majdalani, C. Abecassis-Empis, A. Cowlard, Revisiting the compartment fire, Proceedings of the Eleventh International Symposium, International Association for Fire Safety Science (IAFSS), 10-14 February, Christchurch, New Zealand, 2014, pp. 28–45.

[3] K. Kawagoe, Fire behaviour in rooms, Report No. 27, The Building Research Institute, Tokyo, Japan, 1958.

[4] D. Gross, A.F. Robertson, Experimental fires in enclosures, Symp. (Int.) Combust. 10 (1965) 931–942.

[5] P.H. Thomas, A.J. Heselden, M. Law, Fully-developed Compartment Fires: Two Kinds of Behaviour, Fire Research Technical Paper No. 18, Ministry of Technology and Fire Offices Committee, Joint Fire Research Organization, Fire Research Station, London, England, UK, 1967.

[6] P.H. Thomas, A.J.M. Heselden, Fully-developed fires in single compartments: A co-operative research programme of the Conceil International Du Batiment, Fire Research Note 923, Fire Research Station, Borehamwood, England, UK, 1972.

[7] T.Z. Harmathy, A new look at compartment fires, Part I, Fire Technol. 8 (1972) 196–217.

[8] T.Z. Harmathy, A new look at compartment fires, Part II, Fire Technol. 8 (1972) 326–351.

[9] G. Heskestad, Modeling of enclosure fires, Symp. (Int.) Combust. 14 (1973) 1021–1030.

[10] T.Z. Harmathy, Experimental study on the effect of ventilation on the burning of piles of solid fuels, Combust. Flame. 31 (1978) 259–264.

[11] J.G. Quintiere, B.J. McCaffrey, The burning of wood and plastic cribs in an enclosure: Volume I, NBSIR 80-2054, National Bureau of Standards, Washington DC, USA, 1980.

[12] A. Tewarson, Fully developed enclosure fires of wood cribs, Symp. (Int.) Combust. 20 (1985) 1555–1566.

[13] A.H. Majdalani, J.E. Cadena, A. Cowlard, F. Munoz, J.L. Torero, Experimental characterisation of two fully-developed enclosure fire regimes, Fire Saf. J. 79 (2016) 10–19.

[14] V. Gupta, J.P. Hidalgo, A. Cowlard, C. Abecassis-Empis, A.H. Majdalani, C. Maluk, J.L. Torero, Ventilation effects on the thermal characteristics of fire spread modes in open-plan compartment fires, Fire Saf. J. (2020), https://doi.org/10.1016/j.firesaf.2020.103072.

[15] B.R. Kirby, D.E. Wainman, L.N. Tomlinson, T.R. Kay, B.N. Peacock, Natural fires in large scale compartments – A British Steel Technical, Fire Research Station collaborative project, British Steel Construction, Rotherham, UK, 1994.

[16] K. Horová, T. Jána, F. Wald, Temperature heterogeneity during travelling fire on experimental building, Adv. Eng. Softw. 62–63 (2013) 119–130.

[17] J. Sjöström, E. Hallberg, F. Kahl, A. Temple, J. Andersson, S. Welch, X. Dai, V. Gupta, D. Lange, J.P. Hidalgo, Characterization of TRAvelling FIRes in large compartments, TRAFIR Deliverable Report 2.2, Research Institutes of Sweden, Borås, Sweden, 2019.

[18] J.P. Hidalgo, T. Goode, V. Gupta, A. Cowlard, C. Abecassis-Empis, J. Maclean, A.I. Bartlett, C. Maluk, J.M. Montalvá, A.F. Osorio, J.L. Torero, The Malveira fire test: Full-scale demonstration of fire modes in open-plan compartments, Fire Saf. J. 108 (2019) 102827.

[19] V. Gupta, A.F. Osorio, J.L. Torero, J.P. Hidalgo, Mechanisms of flame spread and burnout in large enclosure fires, Proc. Combust. Inst. (2020), https://doi.org/10.1016/j.proci.2020.07.074.

[20] A. Nadjai, N. Alam, M. Charlier, O. Vassart, X. Dai, J. Franssen, Travelling fire in full scale experimental building subjected to open ventilation conditions, 11th International Conference on Structures in Fire, The University of Queensland, Brisbane, Australia, 2020, pp. 439–450.

[21] M. Heidari, E. Rackauskaite, M. Bonner, E. Christensen, S. Morat, H. Mitchell, P. Kotsovinos, P. Turkowski, W. Wegrzynski, P. Tofilo, G. Rein, Fire experiments inside a very large and open-plan compartment: x-TWO, 11th International Conference on Structures in Fire, The University of Queensland, Brisbane, Australia, 2020, pp. 439–450.

[22] D. Rush, X. Dai, D. Lange, Tisova Fire Test – fire behaviours and lessons learnt, Fire Saf. J. (2020), https://doi.org/10.1016/j.firesaf.2020.103261.

[23] F. Folk, Experiments in fire extinguishment, Natl. Fire Prot. Assoc. Q. 31 (1937) 115–126.

[24] W.L. Fons, Forest Fire Modelling, ASME-ASCE Meeting, Boston, MA, USA, 1963, pp. 164–175.

[25] D. Gross, Experiments on the burning of cross piles of wood, J. Res. Natl. Bur. Stand. 66 (1962) 99–105.

[26] M.J. O'Dogherty, R.A. Young, Miscellaneous experiments on the burning of wooden cribs, Fire Research Note 548, Fire Research Station, Borehamwood, England, UK, 1964.

[27] P.H. Thomas, D.L. Simms, H.G.H. Wraight, Fire spread in wooden cribs - Part II: Heat transfer experiments in still air, Fire Research Note 599, Fire Research Station, Borehamwood, England, UK, 1965.

[28] S. McAllister, M. Finney, Burning Rates of Wood Cribs with Implications for Wildland Fires, Fire Technol. 52 (2016) 1755–1777.

[29] S. McAllister, The Role of Fuel Bed Geometry and Wind on the Burning Rate of Porous Fuels, Front. Mech. Eng. 5 (2019) 1–9.

[30] P.H. Thomas, The Size of Flames from Natural Fires, Symp. (Int.) Combust. 9 (1963) 844–859.

[31] P.H. Thomas, D.L. Simms, H.G.H. Wraight, Fire spread in wooden cribs, Fire Research Note 537, Fire Research Station, Borehamwood, England, UK, 1964.

[32] P.H. Thomas, The contribution of flame radiation to fire spread in forests, Fire Research Note 594, Fire Research Station, Borehamwood, England, UK, 1965.

[33] P.H. Thomas, Some aspects of the growth and spread of fire in the open, Forestry. 40 (1967) 139–164.

[34] P.G. Smith, P.H. Thomas, The rate of burning of wood cribs, Fire Technol. 6 (1970) 29–38.

[35] P.H. Thomas, On the rate of burning of cribs, Fire Research Note 965, Fire Research Station, Borehamwood, England, UK, 1973.

[36] T.Z. Harmathy, The role of thermal feedback in compartment fires, Fire Technol. 11 (1975) 48–54.

[37] J.P. Hidalgo, A. Cowlard, C. Abecassis-Empis, C. Maluk, A.H. Majdalani, S. Kahrmann, R. Hilditch, M. Krajcovic, J.L. Torero, An experimental study of full-scale open floor plan enclosure fires, Fire Saf. J. 89 (2017) 22–40.

[38] J.A. Block, A theoretical and experimental study of nonpropagating free-burning fires, Symp. (Int.) Combust. 13 (1971) 971–978.

[39] M.A. Delichatsios, Fire growth rates in wood cribs, Combust. Flame. 27 (1976) 267–278.

[40] C. Lautenberger, C. Fernandez-Pello, A model for the oxidative pyrolysis of wood, Combust. Flame. 156 (2009) 1503–1513.

[41] R.J. McCarter, A. Broido, Radiative and convective energy from wood crib fires, Pyrodynamics. 2 (1965) 65–85.

[42] W.L. Fons, H.B. Clements, P.M. George, Scale effects on propagation rate of laboratory crib fires, Symp. (Int.) Combust. 9 (1963) 860–866.

[43] P.H. Thomas, D.L. Simms, H.G.H. Wraight, The duration of flaming of wooden sticks in a spreading fire, Fire Research Note 554, Fire Research Station, Borehamwood, England, UK, 1964.

[44] H.W. Emmons, The Film Combustion of Liquid Fuel, ZAMM - J. Appl. Math. Mech. / Zeitschrift Für Angew. Math. Und Mech. 36 (1956) 60–71.

[45] F.J. Kosdon, F.A. Williams, C. Buman, Combustion of vertical cellulosic cylinders in air, Symp. (Int.) Combust. 12 (1969) 253–264.

[46] J.S. Kim, J. de Ris, F. William Kroesser, Laminar free-convective burning of fuel surfaces, Symp. (Int.) Combust. 13 (1971) 949–961.

[47] P.J. Pagni, T.M. Shih, Excess pyrolyzate, Symp. (Int.) Combust. 16 (1977) 1329–1343.

[48] K. Annamalai, M. Sibulkin, Flame spread over combustible surfaces for laminar flow systems Part I: Excess fuel and heat flux, Combust. Sci. Technol. 19 (1979) 167–183.

[49] C. Huggett, Estimation of rate of heat release by means of oxygen consumption measurements, Fire Mater. 4 (1980) 61–65.

[50] J.L. Torero, T. Vietoris, G. Legros, P. Joulain, Estimation of a total mass transfer number from the standoff distance of a spreading flame, Combust. Sci. Technol. 174 (2002) 187–203.

[51] D.B. Spalding, The combustion of liquid fuels, Symp. (Int.) Combust. 4 (1953) 847–864.

[52] A. Tewarson, R.F. Pion, Flammability of plastics-I. Burning intensity, Combust. Flame. 26 (1976) 85–103.

[53] S. Rouvreau, J.L. Torero, P. Joulain, Numerical evaluation of boundary layer assumptions for laminar diffusion flames in microgravity, Combust. Theory Model. 9 (2005) 137–158.

[54] F. Jiang, H. Qi, J.L. de Ris, M.M. Khan, Radiation enhanced B-Number, Combust. Flame. 160 (2013) 1510–1518.

[55] H.C. Hottel, Fire modeling, International Symposium on the Use of Models in Fire Research, National Research Council, Washington DC, USA, 1961, pp. 32–47.

[56] F. Tamanini, A numerical model for the prediction of radiation-controlled turbulent wall fires, Symp. (Int.) Combust. 17 (1979) 1075–1085.

[57] A.S. Rangwala, S.G. Buckley, J.L. Torero, Upward flame spread on a vertically oriented fuel surface: The effect of finite width, Proc. Combust. Inst. 31 (2007) 2607–2615.

[58] T. Vietoris, J.L. Ellzey, P. Joulain, S.N. Mehta, J.L. Torero, Laminar diffusion flame in microgravity: The results of the minitexus 6 sounding rocket experiment, Proc. Combust. Inst. 28 (2000) 2883–2889.

[59] J.L. Consalvi, Y. Pizzo, A. Kaiss, J.L. Torero, B. Porterie, A theoretical and numerical evaluation of the steady-state burning rate of vertically oriented PMMA slabs, Combust. Theory Model. 12 (2008) 451–475.

[60] A.S. Rangwala, S.G. Buckley, J.L. Torero, Analysis of the constant B-number assumption while modeling flame spread, Combust. Flame. 152 (2008) 401–414.

[61] A.V Singh, M.J. Gollner, Steady and transient pyrolysis of a non-charring solid fuel under forced flow, Proc. Combust. Inst. 36 (2017) 3157–3165.

[62] C.H. Bamford, J. Crank, D.H. Malan, The combustion of wood. Part I, Math. Proc. Cambridge Philos. Soc. 42 (1946) 166–182.

[63] P.L. Blackshear, K.A. Murty, Heat and mass transfer to, from, and within cellulosic solids burning in air, Symp. (Int.) Combust. 10 (1965) 911–923.

[64] J.P. Hidalgo, C. Maluk, A. Cowlard, C. Abecassis-Empis, M. Krajcovic, J.L. Torero, A Thin Skin Calorimeter (TSC) for quantifying irradiation during large-scale fire testing, Int. J. Therm. Sci. 112 (2017) 383–394.

[65] R. Emberley, A. Inghelbrecht, Z. Yu, J.L. Torero, Self-extinction of timber, Proc. Combust. Inst. 36 (2017) 3055–3062.

[66] A.I. Bartlett, R.M. Hadden, J.P. Hidalgo, S. Santamaria, F. Wiesner, L.A. Bisby, S. Deeny, B. Lane, Auto-extinction of engineered timber: Application to compartment fires with exposed timber surfaces, Fire Saf. J. 91 (2017).

[67] J. Cuevas, J.L. Torero, C. Maluk, Flame extinction and burning behaviour of timber under varied oxygen concentrations, Fire Saf. J. (2020), https://doi.org/10.1016/j.firesaf.2020.103087.

[68] T.Z. Harmathy, Effect of the nature of fuel on the characteristics of fully developed compartment fires, Fire Mater. 3 (1979) 49–60.

[69] D. Yung, Small-scale compartment fire experiments with PMMA cribs, Fire Saf. J. 17 (1991) 301–313.

[70] T.Z. Harmathy, Mechanism of burning of fully-developed compartment fires, Combust. Flame. 31 (1978) 265–273.

[71] J.G. Quintiere, B.J. McCaffrey, K. Den Braven, Experimental and theoretical analysis of quasi-steady small-scale enclosure fires, Symp. (Int.) Combust. 17 (1979) 1125–1137.

[72] M.L. Bullen, P.H. Thomas, Compartment fires with non-cellulosic fuels, Symp. (Int.) Combust. 17 (1979) 1139–1148.